

Text-image semantic relevance identification for aspect-based multimodal sentiment analysis

TianZhi Zhang¹, Gang Zhou^{Corresp.,1}, Jicang Lu¹, Zhibo Li¹, Hao Wu¹, Shuo Liu¹

¹ Information Engineering University, Zhengzhou, Henan, China

Corresponding Author: Gang Zhou
Email address: gzhougzhou@126.com

Aspect-Based Multimodal Sentiment Analysis (ABMSA) is an emerging task in the research of multimodal sentiment analysis, which aims to identify the sentiment of each given aspect in text and image. Although recent research on ABMSA has achieved some success, most existing models only use attention mechanism to interact aspect with text and image respectively and obtain sentiment output through multimodal concatenation, they often neglect to consider that some samples may not have semantic relevance between text and image. In this paper, we propose a Text-Image Semantic Relevance Identification (TISRI) model for ABMSA to address the problem. Specifically, we introduce a multimodal feature relevance identification module to calculate the semantic similarity between text and image, and then construct an image gate to dynamically control the input image information. On this basis, an image auxiliary information is provided to enhance the semantic expression ability of visual feature representation to generate more intuitive image representation. Furthermore, we finally employ attention mechanism to obtain the text-aware image representation through text-image interaction to prevent irrelevant image information interfering our model. Experiments demonstrate that TISRI achieves competitive results on two ABMSA Twitter datasets, and then validate the effectiveness of our methods.

Text-Image Semantic Relevance Identification for Aspect-Based Multimodal Sentiment Analysis

Tianzhi Zhang¹, Gang Zhou¹, Jicang Lu¹, Zhibo Li¹, Hao Wu, Shuo Liu¹

¹ Information Engineering University, Zhengzhou, Henan, China

Corresponding Author:

Gang Zhou¹

Science Avenue, Zhengzhou, Henan, 450000, China

Email address: gzhougzhou@126.com

Abstract

Aspect-Based Multimodal Sentiment Analysis (ABMSA) is an emerging task in the research of multimodal sentiment analysis, which aims to identify the sentiment of each given aspect in text and image. Although recent research on ABMSA has achieved some success, most existing models only use attention mechanism to interact aspect with text and image respectively and obtain sentiment output through multimodal concatenation, they often neglect to consider that some samples may not have semantic relevance between text and image. In this paper, we propose a Text-Image Semantic Relevance Identification (TISRI) model for ABMSA to address the problem. Specifically, we introduce a multimodal feature relevance identification module to calculate the semantic similarity between text and image, and then construct an image gate to dynamically control the input image information. On this basis, an image auxiliary information is provided to enhance the semantic expression ability of visual feature representation to generate more intuitive image representation. Furthermore, we finally employ attention mechanism to obtain the text-aware image representation through text-image interaction to prevent irrelevant image information interfering our model. Experiments demonstrate that TISRI achieves competitive results on two ABMSA Twitter datasets, and then validate the effectiveness of our methods.

Introduction

With the rapid development of Internet technology, online social and service platforms have gradually become an important part of people's lives (Q. Yu et al., 2019; Fuji and Matsumoto, 2017). Nowadays, the content posted by users is gradually diversified with the prevalence of social media and various service products, and people are more inclined to express their sentiment in multimodal ways such as text and image for different topics and events. Therefore, Multimodal Sentiment Analysis (MSA) task is becoming increasingly important in research communities. Sentiment Analysis (SA) is an effective method to extract valuable information

40 from massive data(Zhu et al., 2022). As an important fine-grained task in sentiment analysis,
41 Aspect-Based Sentiment Analysis (ABSA) has attracted extensive attention from both academia
42 and industry in the past decade for its ability to detect the sentiment polarity of the specific
43 aspect in data(Zhang et al., 2018; Cao and Huang, 2023).

44 Aspect-based Multimodal Sentiment Analysis (ABMSA) is a new subtask of ABSA(Pontiki et
45 al., 2016). In this paper, we introduce image as another modality to assist the text semantic
46 expression, and then predict the sentiment polarity of the aspect involved in text and image.
47 Table 1 shows two representative examples: Table 1(a) chooses “Taylor” as the aspect, the text
48 aims to describe a detail about the event of Taylor’s award, and the smiling face in image also
49 helps to identify the aspect “Taylor” as positive sentiment. Table 1(b) chooses “Percy Harvin”
50 and “JETS” as aspects, the text provides a statement of an objective event and focuses all
51 sentimental expressions on the image, we can infer the aspect “Percy Harvin” as a negative
52 sentiment by his shocked expression in image, but “JETS” as an objectively existing
53 organization has no image reflection, so the aspect “JETS” is assigned a neutral sentiment.
54 Overall, ABMSA is a more refined and challenging task compared with global multimodal
55 sentiment analysis, which can capture the sentiment polarity of text internal entities that cannot
56 be obtained in the global tasks.

57 Given the importance of this field, researchers have proposed numerous methods for ABMSA.
58 For example, Xu et al.(N. Xu et al., 2019) adopted attention mechanism to model interactions
59 between aspect and text, as well as image. Yu et al.(Yu and Jiang, 2019), Yu et al.(J. Yu et al.,
60 2019), and Wang et al.(Wang et al., 2021) further modeled the interactions of text-image, aspect-
61 text, and aspect-image by employing pre-trained language and visual models. These research
62 results demonstrate that integrating image into traditional text sentiment analysis can utilize more
63 comprehensive sentiment information to achieve better sentiment identification effect.

64 Although MSA and ABSA are already popular research fields today, ABMSA is still a relatively
65 new research task. Employing MSA and ABSA research methods to the ABMSA task may
66 present the following challenges: (1) Some samples in dataset have no semantic relevance
67 between text and image. (2) Compared to text, visual feature representation extracted from image
68 is more difficult to perform semantic expression intuitively. (3) In text-relevant images, there
69 may also be regions that are irrelevant to the text semantics and may introduce additional
70 interference to the model.

71 To address the above challenges, we propose a general multimodal architecture named Text-
72 Image Semantic Relevance Identification (TISRI) for ABMSA. Compared with traditional
73 ABMSA models, our main contributions to TISRI are summarized as follows:

74 • To improve the interaction between aspect and text as well as image, we propose a Multimodal
75 Feature Relevance Identification (MFRI) module, which determines the relevance between text
76 and image semantics. Since image is only used as auxiliary information for text here, we
77 construct an image gate to implement dynamic input for image information to prevent irrelevant
78 interference for the model.

- 79 • To enhance the semantic expression of the visual feature representation, we construct an Image
80 Feature Auxiliary Reconstruction (IFAR) layer that introduces Adjective-Noun Pairs (ANPs)
81 extracted from each image in our datasets as image auxiliary information. By fine-tuning the
82 semantic bias between image visual representation and image auxiliary information, we can
83 improve the image visual representation in terms of sentiment from a text level.
- 84 • To prevent the model being influenced by irrelevant image regions, we further interact text and
85 image representation through attention mechanism in the final multimodal feature fusion, and
86 then obtain text-relevant image representation to achieve Image Feature Filtering (IFF).
87 Experimental results demonstrate that TISRI outperforms most existing advanced unimodal and
88 multimodal methods, and achieves competitive results on two ABMSA Twitter datasets.

89

90 **Related Work**

91 Early research on sentiment analysis mainly focused on unimodal sentiment analysis of
92 text(Chen, 2015; Li and Qian, 2016; Shin et al., 2016) and image(You et al., 2017; Li et al.,
93 2018; Wu et al., 2020). In recent years, MSA has gradually become an important focus in
94 sentiment analysis research, and ABMSA has further developed and improved on the basis of
95 ABSA research.

96

97 **Multimodal Sentiment Analysis (MSA)**

98 In recent years, MSA task has attracted widespread attention in academic community(Cambria et
99 al., 2017; Poria et al., 2020), which aims to model text and other non-text modalities (e.g., visual
100 and auditory modalities), and mainly focuses on two subtasks: MSA for conversation and MSA
101 for social media. In MSA for conversation, existing methods mainly focus on adopting different
102 deep learning models (e.g., Long Short-Term Memory Network(Hochreiter and Schmidhuber,
103 1997), Gate Recurrent Unit(Chung et al., 2014), and Transformer(Vaswani et al., 2017)) to
104 model the interaction between different modalities, which have demonstrated better performance
105 in various MSA tasks (e.g., sentiment analysis(Zadeh et al., 2017; Poria et al., 2015, 2017; Liang
106 et al., 2018), emotion analysis(Busso et al., 2004; Lee et al., 2011), and sarcasm detection(Castro
107 et al., 2019; Cai et al., 2019)). In MSA for social media, it mainly includes sentiment analysis of
108 social media image(Chen et al., 2014b; You et al., 2015; Yang et al., 2018a, 2018b) and
109 multimodal sentiment analysis of text-image integration(You et al., 2016; Kumar and Garg,
110 2019; Kumar et al., 2020; Xu et al., 2018). However, the above research methods mainly focus
111 on coarse-grained sentiment analysis (i.e., identifying the global sentiment reflected by each
112 sample) and cannot be directly employed for fine-grained ABMSA tasks.

113

114 **Aspect-Based Sentiment Analysis (ABSA)**

115 As an important fine-grained sentiment analysis task, ABSA has been widely researched and
116 applied in NLP field over the past decade(Cambria et al., 2017), and its current methods can be
117 broadly divided into two categories: discrete feature-based method and deep learning-based
118 method. Discrete feature-based method focuses on designing multi-specific features to train

119 learning classifiers for sentiment analysis(Vo and Zhang, 2015; Pontiki et al., 2016). Deep
120 learning-based method mainly adopts various neural network models to encode aspects and
121 corresponding context information, including the method based on Recursive Neural
122 Network(Dong et al., 2014), Convolutional Neural Network(Xue and Li, 2018), Recurrent
123 Neural Network(Ma et al., 2018; Chen et al., 2017), Attention Mechanism(Wang et al., 2018;
124 Yang et al., 2019; Meškelè and Frasincar, 2020; Zhao et al., 2021), Graph Convolutional
125 Network(Wang et al., 2020; Zhang and Qian, 2020), and pre-trained BERT model that has
126 achieved great success in recent years(H. Xu et al., 2019; Sun et al., 2019). However, the above
127 research methods mainly focus on text-based unimodal information, but do not take into account
128 the fact that relevant information from other modalities (e.g., visual modality) can also contribute
129 to sentiment analysis.

130

131 **Aspect-Based Multimodal Sentiment Analysis (ABMSA)**

132 To conduct research on ABSA utilizing information from different modalities, researchers have
133 developed numerous models for ABMSA over the past three years by employing various
134 effective methods in different tasks. Xu et al.(N. Xu et al., 2019) first explored the ABMSA task
135 and proposed a multi-interactive memory network model MIMN based on BiLSTM for text-
136 image interaction, while also constructed an e-commerce comment dataset for ABMSA. Yu et
137 al.(Yu and Jiang, 2019) proposed an ABMSA model TomBERT based on the BERT
138 architecture, and manually constructed two ABMSA Twitter datasets. Yu et al.(J. Yu et al.,
139 2019) proposed an ABMSA model ESAFN based on entity-sensitive attention and fusion
140 network. Khan et al.(Khan and Fu, 2021) proposed a novel model CapBERT that employs cross-
141 modal transformation to convert the image content into text caption, and performs final
142 sentiment analysis solely based on text modality. Wang et al.(Wang et al., 2021) proposed a
143 recurrent attention network SaliencyBERT also based on BERT, the network effectively captures
144 both intra-modal and inter-modal dynamics by designing a recurrent attention mechanism.
145 Although the above research methods have been validated to be effective in the ABMSA task,
146 they often neglect to identify whether the semantics between modalities are relevant or not. To
147 address this problem, our model captures the semantic relevance between modalities by
148 calculating the similarity between text and image features, which facilitates the effective
149 development of its subsequent work.

150

151 **Methodology**

152 In this chapter, we first formulate our task, and introduce the overall architecture of our Text-
153 Image Semantic Relevance Identification (TISRI) model, then delve into the details of each
154 module in TISRI.

155 **Task Formulation:** Given a set of multimodal samples $D = (x_1, x_2, \dots, x_d)$ as input, each sample
156 $x_i \in D$ contains an m -word text $S = (w_1, w_2, \dots, w_m)$, an associated image I , and an n -word
157 aspect $T = (w_1, w_2, \dots, w_n)$ that is a word subsequence of S . Our task is to predict the sentiment

158 label $y \in Y$ of each given aspect, where Y consists of three categories: positive, negative, and
159 neutral.

160

161 **Overview**

162 Figure 1 illustrates the overall architecture of TISRI, which contains the following modules: (1)
163 Unimodal Feature Extraction Module. (2) Multimodal Feature Relevance Identification Module.
164 (3) Aspect-Multimodal Feature Interaction Module. (4) Multimodal Feature Fusion Module.

165 As shown at the bottom of Fig. 1, for a given multimodal sample, we first extract word feature
166 representations from the input text and aspect, respectively, and visual feature representation
167 from the input image, then aspect representation interacts with text and image representation to
168 generate aspect-aware text representation and aspect-aware image representation.

169 Next, we obtain the semantic similarity between text and image by constructing a multimodal
170 feature relevance identification module. The overall method is shown in Fig. 2, where the fusion
171 representations of text and image are obtained through cross-modal interaction, and then an
172 image gate is constructed in a specific way to dynamically control the input image information.
173 To enable better semantic expression of image feature, we propose an image feature auxiliary
174 reconstruction layer. As shown in Fig. 3, the image visual representation is fine-tuned by
175 introducing Adjective-Noun Pairs (ANPs) extracted from each image in our datasets as image
176 auxiliary information to minimize their representation differences.

177 Finally, to prevent the model being influenced by irrelevant image regions, we interact aspect-
178 aware text representation with aspect-aware image representation, and then generate the final
179 image representation. As shown at the top of Fig. 1, we further concatenate the aspect-aware text
180 representation and the final image representation, and obtain the final sentiment label through a
181 sentiment analysis linear layer.

182

183 **Unimodal Feature Extraction Module**

184 In this module, we adopt two pre-trained models to extract unimodal feature representations from
185 aspect, text and image, respectively.

186

187 **Aspect and Text Representation**

188 Given an input text, we divide it into two parts: aspect T and its corresponding context C , and
189 replace the aspect position in C with a special character “\$T\$”. For text encoding, we employ
190 pre-trained language model RoBERTa(Liu et al., 2019) as the text encoder of our model, which
191 has been proven to achieve competitive performance in various NLP tasks including ABSA(Dai
192 et al., 2021). For T and C , we follow the implementation mechanism of RoBERTa by inserting
193 two special tokens into each input (i.e., “<s>” at the beginning and “</s>” at the end), and then
194 feeding them into text encoder to obtain the hidden representations of aspect:

195 $H_T = \text{RoBERTa}(T)$ and context: $H_C = \text{RoBERTa}(C)$, respectively, where $H_T \in \mathbb{R}^{d \times t}$ and

196 $H_C \in \mathbb{R}^{d \times c}$, d is the hidden dimension, t is the length of aspect, and c is the length of context.

197 Next, we concatenate C with T as sentence S . For S , we use the token “</s>” to separate C
198 from T , and then obtain the hidden representation of sentence: $H_S = \text{RoBERTa}(S)$ through
199 RoBERTa implementation mechanism, where $H_S \in \mathbb{R}^{d \times s}$, $s = c + t$ is the length of sentence. The
200 implementations of aspect, context, and sentence encoding are shown at the bottom of Fig. 1 and
201 Fig. 2.

202 **Image Representation**

204 For image encoding, we employ Residual Network (ResNet)(He et al., 2016) as the image
205 encoder of our model. Compared to the previous VGG network(Simonyan and Zisserman, 2014),
206 ResNet uses residual connections to avoid gradient vanishing problems as the number of layers
207 increases, which allows for deeper extraction of semantic information in image recognition tasks.
208 Specifically, given an input image I , we first resize it to I' with 224×224 pixels, and then take
209 the output of the last convolutional layer in pre-trained 152-layer ResNet as the image visual
210 representation: $H_I = \text{ResNet}(I')$, where $H_I \in \mathbb{R}^{2048 \times 49}$, 49 is the number of visual blocks with the
211 same size by dividing I' into 7×7 , and 2048 is the vector dimension of each visual block.
212 Since we will conduct cross-modal interaction with text and image to obtain the feature
213 representation of text and image fusion, it is necessary to project image representation to the
214 same semantic space as text representation. We employ a linear transformation function for H_I
215 to obtain the final image representation: $H_V = W_I^T H_I$, where $W_I^T \in \mathbb{R}^{2048 \times d}$ is the learnable
216 parameter. The implementation of image encoding is shown at the bottom of Fig. 1.

217 **Multimodal Feature Relevance Identification Module**

219 For images in multimodal samples, while they can provide information beyond text for sentiment
220 analysis, our purpose is to use image to assist in analyzing the sentiment polarity of aspect in
221 text, and images that are irrelevant to text semantics may lead to misalignment of aspects and
222 introduce additional interference to the model. Therefore, we propose a Multimodal Feature
223 Relevance Identification (MFRI) Module, which provides an image gate when integrating text
224 and image, and dynamically controls the input image information based on its relevance to text
225 semantics. MFRI is divided into two layers: (1) Text-Image Cross-Modal Interaction Layer. (2)
226 Image Gate Construction Layer. As shown in Fig. 2, we provide a detailed introduction to the
227 implementation methods of these two layers in the following sections.

228 **Text-Image Cross-Modal Interaction Layer**

230 To better learn sentence feature representation in image, we introduce a multi-head cross-modal
231 attention mechanism (MC-ATT)(Tsai et al., 2019), which treats image representation H_V as
232 query, and sentence representation H_S as key and value, then involves two layer normalization
233 (LN)(Ba et al., 2016) and a feedforward network (FFN)(Vaswani et al., 2017) as follows:

$$234 \quad Z_{V \rightarrow S} = \text{LN}(H_V + \text{MC-ATT}(H_V, H_S)) \quad (1)$$

$$235 \quad H_{V \rightarrow S} = \text{LN}(Z_{V \rightarrow S} + \text{FFN}(Z_{V \rightarrow S})) \quad (2)$$

236 where $H_{V \rightarrow S} \in \mathbb{R}^{d \times 49}$ is the image-aware sentence representation generated by MC-ATT layer.

237 However, image representation is treated as query in the above MC-ATT layer, and each vector
238 in the generated $H_{V \rightarrow S}$ represents a visual block rather than a word representation in sentence.

239 We expect that image-aware sentence representation can reflect on each word in sentence. Given
240 this problem, we introduce another MC-ATT layer that treats H_S as query, and $H_{V \rightarrow S}$ as key
241 and value, then generates the final image-aware sentence representation $H'_{V \rightarrow S}$, where

$$242 \quad H'_{V \rightarrow S} \in \mathbb{R}^{d \times s}.$$

243 To obtain the image representation for each word in sentence, we adopt the same method as
244 above for cross-modal interaction, treating H_S as query, and H_V as key and value, then

245 generating the sentence-aware image representation $H_{S \rightarrow V}$, where $H_{S \rightarrow V} \in \mathbb{R}^{d \times s}$.

246

247 **Image Gate Construction Layer**

248 Yu et al.(Yu et al., 2020) introduced visual gate to dynamically control the contribution of image
249 visual features to each word in text in the multimodal named entity recognition work and
250 achieved effective experimental results. Inspired by this work, we construct a gate for the input
251 image information, which is responsible for dynamically controlling the contribution of image
252 information in our model by assigning a weight in $[0,1]$ to each image based on its relevance to
253 corresponding sentence, preserving the higher relevance image by assigning a higher weight, and
254 filtering the lower relevance image by assigning a lower weight. Specifically, we first
255 concatenate $H'_{V \rightarrow S}$ and $H_{S \rightarrow V}$, and then construct the gate based on text-image relevance weight
256 through linear transformation and nonlinear activation function:

$$257 \quad g = \sigma(W_{S \rightarrow V}[H'_{V \rightarrow S}; H_{S \rightarrow V}]) \quad (3)$$

258 where $W_{S \rightarrow V} \in \mathbb{R}^{d \times 2d}$ is the learnable parameter, σ is the element-wise nonlinear activation
259 function, which is used to control the output of g in $[0,1]$.

260 Based on the above image gate g , we can obtain the final image representation that assigns
261 relevance weight:

$$262 \quad H'_V = g \cdot H_{S \rightarrow V} \quad (4)$$

263

264 **Aspect-Multimodal Feature Interaction Module**

265 After obtaining the feature representations of aspect, context, and image, we analyze the
266 relationships between aspect and image as well as context, respectively. Furthermore, we design
267 an Image Feature Auxiliary Reconstruction (IFAR) Layer, which serves as an auxiliary
268 supervision for visual representation. The specific technical scheme of this module is shown at
269 the middle part of Fig. 1, and the internal architecture of IFAR Layer is shown in Fig. 3. We
270 provide a detailed implementation methods for them in the following sections.

271

272 **Aspect Interaction Layer**

273 The main purpose of this layer is to obtain aspect-aware image representation and aspect-aware
 274 context representation, so we employ MC-ATT layer to interact with aspect and image as well as
 275 context, respectively, to promote information integration between modalities. Specifically, we
 276 first conduct cross-modal feature interaction between aspect and image, treating aspect
 277 representation H_T as query, and image representation H_V as key and value:

$$278 \quad Z_{T \rightarrow V} = \text{LN}(H_T + \text{MC-ATT}(H_T, H_V)) \quad (5)$$

$$279 \quad H_{T \rightarrow V} = \text{LN}(Z_{T \rightarrow V} + \text{FFN}(Z_{T \rightarrow V})) \quad (6)$$

280 where $H_{T \rightarrow V} \in \mathbb{R}^{d \times t}$ is the aspect-aware image representation generated by MC-ATT layer.

281 Similarly, we can also obtain the aspect-aware context representation $H_{T \rightarrow C}$, where $H_{T \rightarrow C} \in \mathbb{R}^{d \times t}$

282 .

283

284 **Image Feature Auxiliary Reconstruction Layer**

285 To improve the effectiveness of visual feature representation, we introduce Adjective-Noun Pairs
 286 (ANPs) extracted from the image in each sample. Since the nouns and adjectives in ANPs can
 287 reflect real content and sentiment in image to some extent, we employ them as auxiliary
 288 supervision for visual representation to obtain a more intuitive image semantic expression.
 289 Specifically, we adopt DeepSentiBank(Chen et al., 2014a) to generate 2089 ANPs for each
 290 image and select the top k ANPs as image auxiliary information.

291 However, the extraction of image ANPs is essentially a coarse-grained extraction method, so
 292 extracted ANPs may be the content of image regions that are irrelevant to aspect or may be
 293 semantic information that is incorrectly recognized for image, and directly using these ANPs can
 294 significantly introduce additional interference to the model due to their inaccuracy. Zhao et
 295 al.(Zhao et al., 2022) obtained nouns relevant to aspect by calculating semantic similarity
 296 between aspect representation and ANPs noun representation in the construction of ABMSA
 297 knowledge enhancement framework, and achieved excellent alignment effect in their
 298 experiment. Inspired by this work, we concatenate the above k ANPs and their corresponding
 299 nouns, respectively, and feed them into text encoder to obtain the ANPs representation H_{ANPs}
 300 and the noun representation H_N , and then we employ cosine similarity to calculate the semantic
 301 similarity between H_T and H_N to achieve the aspect alignment:

$$302 \quad \alpha = \frac{H_T^T \cdot H_N}{\|H_T\| \cdot \|H_N\|} \quad (7)$$

303 where α is the similarity score between H_T and H_N , which we use as a weight vector
 304 representing the semantic relevance of ANPs to the aspect expressed in image. Next, we assign
 305 each individual in ANPs representation with its corresponding relevance weight to obtain the
 306 image auxiliary information representation:

$$307 \quad H'_{ANPs} = \alpha \cdot H_{ANPs} \quad (8)$$

308 Furthermore, based on the construction of image gate g in the above Multimodal Feature
309 Relevance Identification Module, we also treat g as image auxiliary information gate to
310 dynamically control the contribution of ANPs to the model, and then obtain the final image
311 auxiliary information representation:

$$312 \quad H''_{ANPs} = g \cdot H'_{ANPs} \quad (9)$$

313 To enable visual attention to be more intuitive and accurate in representing the visual features of
314 aspect in image, we introduce a reconstruction loss function based on mean square error (MSE)
315 to minimize the difference between aspect-aware image representation $H_{T \rightarrow V}$ and final image
316 auxiliary information representation H''_{ANPs} :

$$317 \quad L_R = \frac{1}{|D|} \sum_{i=1}^{|D|} (H''_{ANPs} - H_{T \rightarrow V})^2 \quad (10)$$

318 **Multimodal Feature Fusion Module**

319 In this module, we fuse aspect-aware context representation $H_{T \rightarrow C}$ and aspect-aware image
320 representation $H_{T \rightarrow V}$ with our Image Feature Filtering (IFF) method to obtain the final aspect
321 output representation. The implementation is shown at the top of Fig. 1. First, we employ MC-
322 ATT to implement the interaction between $H_{T \rightarrow C}$ and $H_{T \rightarrow V}$ to obtain the visual feature
323 representation corresponding to aspect-aware context in aspect-aware image as the final aspect-
324 aware image representation, and then filter the irrelevant regions in image:

$$325 \quad Z_{T \rightarrow C \rightarrow V} = \text{LN}(H_{T \rightarrow C} + \text{MC-ATT}(H_{T \rightarrow C}, H_{T \rightarrow V})) \quad (11)$$

$$326 \quad H_{T \rightarrow C \rightarrow V} = \text{LN}(Z_{T \rightarrow C \rightarrow V} + \text{FFN}(Z_{T \rightarrow C \rightarrow V})) \quad (12)$$

327 Next, we concatenate $H_{T \rightarrow C}$ and $H_{T \rightarrow C \rightarrow V}$, and then feed them into a multimodal self-attention
328 layer based on Transformer for feature fusion between modalities:

$$329 \quad H = \text{Transformer}(H_{T \rightarrow C}; H_{T \rightarrow C \rightarrow V}) \quad (13)$$

330 Finally, we feed the first token representation H^0 into Softmax layer to obtain the final
331 sentiment label:

$$332 \quad P(y|H) = \text{Softmax}(W^T H^0) \quad (14)$$

333 We adopt the cross entropy loss constructed by predicted values of aspect-based sentiment labels
334 and their true values as the training loss function for model sentiment analysis task:

$$335 \quad L_S = \frac{1}{|D|} \sum_{j=1}^{|D|} \log P(y^j | H^0) \quad (15)$$

336 To further optimize all parameters of our model, we train the loss function for sentiment analysis
337 jointly with image auxiliary reconstruction, and then construct a final training loss function
338 combining the two tasks:
339

$$L = L_S + \lambda L_R \quad (16)$$

Where λ is the tradeoff hyper-parameter used to control the contribution of reconstruction loss.

342

343 Experiment

344 In this chapter, we conduct extensive experiments on two ABMSA datasets to validate the
345 effectiveness of our Text-Image Semantic Relevance Identification (TISRI) model.

346

347 Experimental Settings

348 **Datasets:** We adopt two benchmark datasets of ABMSA TWITTER-2015 and TWITTER-2017
349 proposed by Yu et al.(Yu and Jiang, 2019) that are composed of multimodal tweets posted on
350 TWITTER in 2014-2015 and 2016-2017, where each sample consists of a text, an image, a given
351 aspect, and the sentiment label (positive, negative, and neutral) corresponding to the aspect. The
352 relevant information of these two datasets is shown in Table 2.

353 **Implementation Details:** For TISRI, we adopt RoBERTa-base(Liu et al., 2019) as the encoder
354 for sentence, context, and aspect in text, and ResNet-152(He et al., 2016) as the image encoder.
355 During alternating optimization process, we use AdamW as the learner to optimize parameters.
356 Specifically, we set the batch size to 16, the training epoch to 9, the k value to 5, the λ value to
357 0.8, the model learning rate to $1e-5$, the maximum length of sentence and context to 128, the
358 maximum length of aspect to 32, and the hidden dimension to 768. We demonstrate the average
359 results of three independent training runs for all our models. All the models are implemented
360 based on PyTorch, and run on an NVIDIA Tesla V100 GPU.

361

362 Compared Baselines

363 In this section, we evaluate the performance of TISRI by comparing it with various existing
364 methods. Specifically, we consider comparing the following unimodal and multimodal methods
365 to our model:

- 366 • Res-Target: a baseline method for obtaining the visual feature representation of input image
367 directly from the ResNet model.
- 368 • AE-LSTM(Wang et al., 2016): an attention-based LSTM model for obtaining important
369 context relevant to aspect.
- 370 • MGAN(Fan et al., 2018): a multi-grained attention network that fuses aspect and context at
371 different granularity.
- 372 • BERT(Devlin et al., 2018): a pre-trained language model with stacked Transformer encoder
373 layers for the interaction between aspect and text.
- 374 • RoBERTa(Liu et al., 2019): further improvement of BERT model by adopting better training
375 strategies and larger corpus.
- 376 • MIMN(N. Xu et al., 2019): a multi-interactive memory network for the interaction between
377 aspect, text, and image.

- 378 • ESAFN(J. Yu et al., 2019): an entity-sensitive attention and fusion network for obtaining inter-
379 modal dynamics of aspect, text, and image.
- 380 • ViLBERT(Lu et al., 2019): a pre-trained visual language model that takes aspect-text pairs as
381 input text.
- 382 • TomBERT(Yu and Jiang, 2019): an aspect-aware ABMSA method based on multimodal
383 BERT model architecture.
- 384 • SaliencyBERT(Wang et al., 2021): a recursive attention network based on multimodal BERT
385 model architecture for ABMSA.
- 386 • CapBERT(Khan and Fu, 2021): a method of converting image into text caption and feeding it
387 with the input text to a pre-processed BERT model.
- 388 • KEF-TomBERT(Zhao et al., 2022): an extended baseline to apply a proposed knowledge
389 enhancement framework KEF to TomBERT.
- 390 • KEF-SaliencyBERT(Zhao et al., 2022): an extended baseline to apply a proposed knowledge
391 enhancement framework KEF to SaliencyBERT.
- 392 • CapRoBERTa: an extended baseline that replaces BERT with RoBERTa in CapBERT.
- 393 • KEF-TomRoBERTa: an extended baseline that replaces BERT with RoBERTa in KEF-
394 TomBERT.

395

396 **Experimental Results and Analysis**

397 Table 3 demonstrates the performance of our model and each compared baseline model on
398 TWITTER-2015 and TWITTER-2017 datasets. We adopt Accuracy (Acc) and Macro-F1 as
399 evaluation metrics and mark the best score for each metric in bold. As shown at the last five
400 columns of Table 3, we compare our model with the latest proposed best performing KEF-
401 TomBERT and KEF-SaliencyBERT last year. In addition, we also select the best performing
402 CapBERT from original baseline model and better performing KEF-TomBERT from the above
403 two models, and replace the BERT in them with RoBERTa to implement a more comprehensive
404 and fair comparison of TISRI.

405 Based on all the experimental results in Table 3, we can conclude as follows: (1) The
406 performance of Res-Target is lower than that of all text language models, which may be
407 explained by the fact that image relevant to aspect mostly serve as an auxiliary role for text and
408 do not perform well as an independent modality for sentiment prediction. (2) Most multimodal
409 methods generally perform better than unimodal methods, which indicates that image
410 information can complement text information to obtain a higher sentiment prediction ability. (3)
411 TomBERT, SaliencyBERT and CapBERT perform much better than other multimodal models,
412 and we speculate that adopting multi-head cross-modal attention with self-attention mechanism
413 to do cross-modal interaction on aspect can obtain more robust feature representation. (4) Among
414 all original baseline models, CapBERT achieves the best performance due to image caption,
415 which indicates that text has a more intuitive semantic representation than image. (5) The
416 performance of KEF-TomBERT and KEF-SaliencyBERT is better than that of other original

417 baseline models, which indicates that the knowledge enhancement framework KEF can improve
418 the performance of original model by introducing image adjective and noun information to some
419 extent and has excellent compatibility effect. (6) Since RoBERTa is more powerful than BERT,
420 intuitively the overall performance of CapRoBERTa is generally better than that of CapBERT on
421 the above evaluation metrics. (7) Compared to the best performing KEF-TomRoBERTa, our
422 model achieves competitive results on the two datasets, which has about 0.5% higher Macro-F1
423 on TWITTER-2015 dataset, and about 0.4% and 1.2% higher Accuracy and Macro-F1 on
424 TWITTER-2017 dataset, respectively.

425 For the slightly lower accuracy of our model on TWITTER-2015 dataset compared to KEF-
426 TomRoBERTa, we speculate that the possible reason is that KEF-TomRoBERTa applies
427 adjectives in the obtained ANPs directly to aspect-aware image representation, while the overall
428 text-image relevance weights on TWITTER-2015 dataset may be relatively higher than those on
429 TWITTER-2017 dataset, which is also validated in the TISRI w/o MFRI part of ablation study in
430 Section 4.4. Therefore, the direct use of adjectives in this case can express the sentiment in
431 image more intuitively to some extent. However, for the condition where ANPs identify
432 semantic error in image or text-image relevance has a low weight, KEF-TomRoBERTa may
433 introduce additional interference to the model by directly using irrelevant adjectives. Overall, we
434 speculate that TISRI performs better on TWITTER-2017 dataset for this reason.

435

436 **Ablation Study**

437 To further investigate the impact of individual unit in TISRI on model performance, we perform
438 ablation analysis on TWITTER-2015 and TWITTER-2017 datasets for several important units in
439 the model: (1) Image Feature Filtering (IFF) method. (2) Image Feature Auxiliary
440 Reconstruction (IFAR) Layer. (3) Multimodal Feature Relevance Identification (MFRI) Module.
441 We first remove the above three units respectively, and then remove these units at the same time
442 leaving only the bone framework, so we can have a clearer and more comprehensive
443 understanding of the contribution of individual unit to the model performance improvement. The
444 experimental results are shown in Table 4, where w/o represents the removal of the
445 corresponding unit.

446 First, we can learn that removing IFF unit decreases Accuracy by about 1.9% and 1.5% on the
447 two datasets, respectively, which validates that retaining useful information in image and
448 implementing filtering on text-irrelevant image regions helps reduce the impact of interference
449 on model performance. Next, removing IFAR unit decreases Accuracy by about 2.1% and 2.5%
450 on the two datasets, respectively, which proves that the unit has a large contribution to model
451 performance improvement and validates that adopting ANPs as image auxiliary information can
452 be more intuitive for semantic expression of visual feature representation. Then, removing the
453 MFRI unit decreases Accuracy by about 0.7% and 1.8% on the two datasets, respectively, which
454 validates that assigning image to an inter-modal relevance weight can help to prevent additional
455 interference to the model from text-irrelevant images. We can also learn that there are more
456 images with higher text-image relevance weights in TWITTER-2015 dataset than in TWITTER-

457 2017 dataset, which validates the reason we inferred in Section 4.3. Finally, we remove all above
458 units and observe that Accuracy decreases by about 2.2% and 4.5% on the two datasets,
459 respectively, which validates the effectiveness of our proposed units in the model and also
460 validates that these units contribute to model performance improvement to some extent from
461 another perspective.

462

463 **Parameter Analysis**

464 In this section, we provide a detailed introduction and analysis of the process of evaluating
465 optimal hyper-parameters. All of the above experiments are set based on optimized model hyper-
466 parameters.

467

468 **Values of Epoch and Batch Size**

469 To analyze the impact of different epoch and batch size on model performance, we determine the
470 final values of epoch and batch size through experiments in this subsection. Figure 4 and Figure
471 5 demonstrate the model performance of different epoch and batch size values on the two
472 datasets, respectively, and we can draw the following inferences. First, we experiment with the
473 value of epoch. We find that as the value of epoch increases, model performance shows an
474 upward trend and then gradually stabilizes. The model performance is optimal when epoch
475 equals 8, and then Accuracy and Macro-F1 of the model start to gradually decrease when epoch
476 equals 9. Thus, we set the value of epoch to 9 in experiment. Accuracy and Macro-F1
477 corresponding to the epoch setting of TISRI on TWITTER-2015 and TWITTER-2017 datasets
478 are shown in Fig. 4(a) and Fig. 4(b).

479 Then, we analyze the value of batch size using 8, 16 and 32, respectively, and experimental
480 results on the two datasets are shown in Fig. 5(a) and Fig. 5(b). We can clearly find that the
481 model achieves the best performance on both datasets when batch size equals 16. The possible
482 reasons are speculated as follows: When batch size equals 8, it is small for the number of
483 samples in the two datasets, and the training of model is not only time-consuming but also
484 difficult to converge, which leads to the underfitting of model. In a certain range, the increase of
485 batch size is conducive to the stability of model convergence. However, when batch size equals
486 32, the model may fall into local minimum because it is too large, which leads to the
487 deterioration of model generalization performance. Thus, we set the value of batch size to 16 in
488 experiment.

489

490 **Value of k**

491 To explore the impact of ANPs on model performance, we extract the top k ANPs for each
492 image where k is set as each integer in $[1,10]$, and take values for them respectively to
493 experiment. Figure 6(a) and Figure 6(b) demonstrate the model performance of k value on the
494 two datasets, respectively, and we can draw the following inferences. First, the model
495 performance is poor without ANPs as image auxiliary information, which indicates that
496 combining ANPs can improve the performance of TISRI. Second, the model performance shows

497 a fluctuating upward trend as the number of ANPs increases and reaches the best state when k
498 equals 5. However, the model performance no longer improves but shows a trend of decline
499 when k is greater than 5. The possible reason is speculated as follows: The number of aspects
500 involved in each text in the two datasets may not exceed 5, and when k is greater than it, image
501 auxiliary information may introduce additional interference to the model. Therefore, we set the
502 value of k to 5 in experiment.

503

504 **Value of λ**

505 To investigate the effect of trade-off hyper-parameter λ that controls the auxiliary reconstruction
506 loss contribution of IFAR layer on model performance, we set λ to a decimal number with an
507 interval of 0.1 in the range of [0,1] to experiment. Figure 7(a) and Figure 7(b) demonstrate the
508 model performance of λ value on the two datasets, respectively. The model performance shows
509 a fluctuating upward trend as λ increases, which has a more obvious effect on TWITTER-2017
510 dataset. When λ equals 0.8, the model performance reaches the best state, and then decreases
511 gradually as λ increases. We speculate that the possible reason is that ANPs as image auxiliary
512 information only serve to improve the semantic expression of image visual features. When the
513 trade-off hyper-parameter λ exceeds a certain value, image auxiliary information plays a
514 dominant role in image representation, but these ANPs may have semantic information of image
515 recognition error, so the model will largely introduce additional interference when λ is too large
516 and produce negative effect. Thus, we set the trade-off hyper-parameter λ to 0.8 in the error
517 back propagation process.

518

519 **Case Study**

520 In this section, we provide an in-depth analysis of the results of different models on TWITTER-
521 2015 and TWITTER-2017 datasets to better understand the advantages of our model.
522 Specifically, we first select four samples from test datasets to compare the sentiment prediction
523 performance of TISRI with other models, and then screen the samples for error analysis in TISRI
524 and analyze the possible causes of their errors.

525

526 **Prediction Results**

527 Table 5 demonstrates the comparison results of the sentiment prediction performance of three
528 models RoBERTa, CapRoBERTa, and TISRI on four samples where we have an advantage.
529 Since our model uses image gate and ANPs to assist with image information, we demonstrate
530 them in the table as well. Table 5(a) demonstrates that image has a higher relevance weight with
531 text, and the noun “team” associated with the aspect “Thunder” in ANPs has positive words
532 “excellent” and “victorious” as modifiers, so our model can accurately predict the sentiment
533 polarity as positive, while CapRoBERTa gives a wrong prediction. In Table 5(b), the image also
534 has a higher relevance weight with text, and the ANPs contain positive words such as
535 “handsome” and “smile”, so our model also makes correct prediction, while CapRoBERTa
536 predicts a wrong sentiment label. However, the image content in Table 5(c) is relatively

537 complex, and old black and white photo also has certain limitations in image recognition, so the
538 text-image relevance weight is not high. Fortunately, the ANPs identify nouns such as “team”
539 relevant to image content, and also have positive adjectives like “successful” as noun modifiers,
540 so our model successfully predict correct sentiment label, while RoBERTa and CapRoBERTa
541 give wrong predictions. In Table 5(d), the text-image relevance weight is slightly lower than the
542 other three samples because the text is too short and less relevant to image content, but the ANPs
543 have several positive words such as “hot”, “pretty”, and “sexy”, which help our model to make
544 accurate prediction from another perspective, while CapRoBERTa predicts a wrong sentiment
545 label.

546 However, we find that multimodal CapRoBERTa model makes all wrong predictions in these
547 four samples, while unimodal RoBERTa model makes only one wrong prediction, which is
548 unreasonable from model interpretability perspective. Through investigation, we learn that the
549 image caption in Table 5(a) is “A man in a tennis outfit is jumping in the air.”, Table 5(b) is “A
550 woman with a tie and a flower in her hand.”, Table 5(c) is “A group of baseball players standing
551 next to each other.” and Table 5(d) is “Two women in a field with a dog.”. We find that these
552 captions not only contain incorrect recognition, but fail to reflect the adjectives or nouns relevant
553 to facial expression in Table 5(b) and Table 5(d). Furthermore, CapRoBERTa completely relies
554 on image caption to obtain image representation but discards original image information, so it
555 cannot accurately reflect the sentiment embodied in image to some extent, and then affect the
556 final sentiment prediction.

557

558 **Error Analysis**

559 On the basis of the above experiments, we further perform error analysis on TISRI to deepen our
560 understanding of model performance. Table 6 demonstrates three types of error prediction
561 examples, including the following categories: (1) The ANPs are incorrect in image semantic
562 recognition. (2) The aspect in text cannot find nouns with high similarity in ANPs. (3) The model
563 cannot recognize deeper sentiment in text and image. First, the ANPs in Table 6(a) incorrectly
564 recognize image semantics. For an image that does not reflect any positive sentiment, its ANPs
565 produce positive words such as “laughing” and “funny” that completely hinder correct sentiment
566 recognition, so the image representation is affected by these words. Then, the aspect “WILD
567 Women” in Table 6(b) is actually an organization name. Since it cannot be represented
568 intuitively in image causing ANPs recognizing some aspect-irrelevant nouns, the image cannot
569 accurately express the sentiment semantics of aspect. Finally, the text in Table 6(c) states an
570 objective event that Martin St. Louis announced his retirement, and the image demonstrates a
571 moment he waved his hand on the field. However, our model can only identify semantic features
572 on the surface of text and image but cannot feel Martin's unwillingness to leave the stadium, so
573 this problem is also the difficulty for TISRI to further intelligently identify sentiment in the
574 future.

575

576 **Conclusions**

577 In this paper, we propose an Aspect-Based Multimodal Sentiment Analysis (ABMSA) model
578 TISRI. First, the model calculates text-image semantic relevance and constructs an image gate
579 that dynamically controls the input of image information. Then, it introduces Adjective-Noun
580 Pairs (ANPs) as image auxiliary information to enhance the semantic expression ability of image
581 visual features. Finally, we adopt attention mechanism to interact with text and image
582 representation to obtain filtered text-relevant image representation for the final sentiment
583 prediction. Experimental results demonstrate that our proposed model outperforms the majority
584 of existing advanced models on TWITTER-2015 dataset and all compared baseline models on
585 TWITTER-2017 dataset, and validate the superiority of our model and the effectiveness of our
586 methods.

587 We plan to expand our future research in the following directions. First, we aim to apply TISRI
588 to more multimodal related tasks, where our inter-modal feature relevance identification and
589 image feature auxiliary semantic enhancement units can be easily extended to other tasks such as
590 multimodal event extraction and multimodal named entity recognition. Moreover, with the
591 prevalence of large model, we aim to further explore how to effectively integrate large model
592 into our work and achieve more specific multiclassification tasks in subsequent research.

593

594 **Acknowledgements**

595 This research is supported by the Science and Technology Research Program of the Department
596 of Science and Technology of Henan Province (approval No.: 222102210081)

597

598 **References**

- 599 Yu Q, Zhou J, Gong W. 2019. A lightweight sentiment analysis method. *ZTE Communications*
600 17: 2–8. DOI: 10.12142/ZTECOM.201903002.
- 601 Fuji R, Matsumoto K. 2017. Emotion analysis on social big data. *ZTE Communications* 15: 30–
602 37. DOI: 10.3969/j.issn.1673-5188.2017.S2.005.
- 603 Zhu L, Xu M, Bao Y, Xu Y, Kong X. 2022. Deep learning for aspect-based sentiment analysis: a
604 review. *PeerJ Computer Science* 8: e1044. DOI: 10.7717/peerj-cs.1044.
- 605 Zhang L, Wang S, Liu B. 2018. Deep learning for sentiment analysis: A survey. *Wiley*
606 *Interdisciplinary Reviews: Data Mining and Knowledge Discovery* 8: e1253. DOI:
607 10.1002/widm.1253
- 608 Cao F, Huang X. 2023. Performance analysis of aspect-level sentiment classification task based
609 on different deep learning models. *PeerJ Computer Science* 9: e1578. DOI: 10.7717/peerj-
610 cs.1578.
- 611 Pontiki M, Galanis D, Papageorgiou H, Androutsopoulos I, Manandhar S, Al-Smadi M, Al-
612 Ayyoub M, Zhao Y, Qin B, De Clercq O. 2016. Semeval-2016 task 5: Aspect based sentiment
613 analysis. In: *ProWorkshop on Semantic Evaluation (SemEval-2016)*. 19–30. DOI:
614 10.18653/v1/S16-1002.

- 615 Xu N, Mao W, Chen G. 2019. Multi-interactive memory network for aspect based multimodal
616 sentiment analysis. In: *Proceedings of the AAAI Conference on Artificial Intelligence*. 371–378.
617 DOI: 10.1609/aaai.v33i01.3301371.
- 618 Yu J, Jiang J. 2019. Adapting BERT for target-oriented multimodal sentiment classification. In:
619 *Proceedings of the Twenty-Eighth International Joint Conference on Artificial Intelligence*
620 *Main track*. 5408-5414. DOI: 10.24963/ijcai.2019/751.
- 621 Yu J, Jiang J, Xia R. 2019. Entity-sensitive attention and fusion network for entity-level
622 multimodal sentiment classification. *IEEE/ACM Transactions on Audio, Speech, and Language*
623 *Processing* 28: 429–439. DOI: 10.1109/TASLP.2019.2957872.
- 624 Wang J, Liu Z, Sheng V, Song Y, Qiu C. 2021. Saliencybert: Recurrent attention network for
625 target-oriented multimodal sentiment classification. In: *Pattern Recognition and Computer*
626 *Vision: 4th Chinese Conference, PRCV 2021, Beijing, China, October 29–November 1, 2021,*
627 *Proceedings, Part III 4*. Springer. 3–15. DOI: 10.1007/978-3-030-88010-1_1.
- 628 Chen Y. 2015. Convolutional Neural Network for Sentence Classification. *University of*
629 *Waterloo*.
- 630 Li D, Qian J. 2016. Text sentiment analysis based on long short-term memory. In: *2016 First*
631 *IEEE International Conference on Computer Communication and the Internet (ICCCI)*. 471–
632 475. DOI: 10.1109/CCI.2016.7778967.
- 633 Shin B, Lee T, Choi J.D. 2016. Lexicon integrated CNN models with attention for sentiment
634 analysis. In: *Proceedings of the 8th Workshop on Computational Approaches to Subjectivity,*
635 *Sentiment and Social Media Analysis*. 149-158. DOI: 10.18653/v1/W17-5220.
- 636 You Q, Jin H, Luo J. 2017. Visual sentiment analysis by attending on local image regions. In:
637 *Proceedings of the AAAI Conference on Artificial Intelligence*. 31(1). DOI:
638 10.1609/aaai.v31i1.10501.
- 639 Li Z, Fan Y, Liu W, Wang F. 2018. Image sentiment prediction based on textual descriptions
640 with adjective noun pairs. *Multimedia Tools and Applications* 77: 1115–1132. DOI:
641 10.1007/s11042-016-4310-5.
- 642 Wu L, Qi M, Jian M, Zhang H. 2020. Visual sentiment analysis by combining global and local
643 information. *Neural Processing Letters* 51: 2063–2075. DOI: 10.1007/s11063-019-10027-7.
- 644 Cambria E, Das D, Bandyopadhyay S, Feraco A. 2017. Affective computing and sentiment
645 analysis. *A practical guide to sentiment analysis*. 1–10. DOI: 10.1109/MIS.2016.31.
- 646 Poria S, Hazarika D, Majumder N, Mihalcea R. 2020. Beneath the tip of the iceberg: Current
647 challenges and new directions in sentiment analysis research. *IEEE Transactions on Affective*
648 *Computing*. 108 - 132. DOI: 10.1109/TAFFC.2020.3038167.
- 649 Hochreiter S, Schmidhuber J. 1997. Long short-term memory. *Neural computation* 9: 1735–
650 1780. DOI: 10.1162/neco.1997.9.8.1735.
- 651 Chung J, Gulcehre C, Cho K, Bengio Y. 2014. Empirical evaluation of gated recurrent neural
652 networks on sequence modeling. *arXiv preprint arXiv:1412.3555*.

- 653 Vaswani A, Shazeer N, Parmar N, Uszkoreit J, Jones L, Gomez A.N, Kaiser Ł, Polosukhin I.
654 2017. Attention is all you need. *Advances in neural information processing systems*. 6000–6010.
655 DOI: 10.5555/3295222.3295349.
- 656 Zadeh A, Chen M, Poria S, Cambria E, Morency L-P. 2017. Tensor fusion network for
657 multimodal sentiment analysis. In: *Proceedings of the 2017 Conference on Empirical Methods in*
658 *Natural Language Processing*. 1103–1114. DOI: 10.18653/v1/D17-1115.
- 659 Poria S, Cambria E, Gelbukh A. 2015. Deep convolutional neural network textual features and
660 multiple kernel learning for utterance-level multimodal sentiment analysis. In: *Proceedings of*
661 *the 2015 Conference on Empirical Methods in Natural Language Processing*. 2539–2544. DOI:
662 10.18653/v1/D15-1303.
- 663 Poria S, Cambria E, Hazarika D, Majumder N, Zadeh A, Morency L-P. 2017. Context-dependent
664 sentiment analysis in user-generated videos. In: *Proceedings of the 55th Annual Meeting of the*
665 *Association for Computational Linguistics (Volume 1: Long Papers)*. 873–883. DOI:
666 10.18653/v1/P17-1081.
- 667 Liang PP, Liu Z, Zadeh A, Morency L-P. 2018. Multimodal language analysis with recurrent
668 multistage fusion. In: *Proceedings of the 2018 Conference on Empirical Methods in Natural*
669 *Language Processing*. 150-161. DOI: 10.18653/v1/D18-1014.
- 670 Busso C, Deng Z, Yildirim S, Bulut M, Lee CM, Kazemzadeh A, Lee S, Neumann U, Narayanan
671 S. 2004. Analysis of emotion recognition using facial expressions, speech and multimodal
672 information. In: *Proceedings of the 6th International Conference on Multimodal Interfaces*. 205–
673 211. DOI: 10.1145/1027933.1027968.
- 674 Lee C-C, Mower E, Busso C, Lee S, Narayanan S. 2011. Emotion recognition using a
675 hierarchical binary decision tree approach. *Speech Communication*. 53(9-10): 1162-1171. DOI:
676 10.1016/j.specom.2011.06.004.
- 677 Castro S, Hazarika D, Pérez-Rosas V, Zimmermann R, Mihalcea R, Poria S. 2019. Towards
678 multimodal sarcasm detection (an _obviously_ perfect paper). In: *Proceedings of the 57th*
679 *Annual Meeting of the Association for Computational Linguistic*. 4619-4629. DOI:
680 10.18653/v1/P19-1455.
- 681 Cai Y, Cai H, Wan X. 2019. Multi-modal sarcasm detection in twitter with hierarchical fusion
682 model. In: *Proceedings of the 57th Annual Meeting of the Association for Computational*
683 *Linguistics*. 2506–2515. DOI: 10.18653/v1/P19-1239.
- 684 Chen T, Yu FX, Chen J, Cui Y, Chen Y-Y, Chang S-F. 2014b. Object-based visual sentiment
685 concept analysis and application. In: *Proceedings of the 22nd ACM International Conference on*
686 *Multimedia*. 367–376. DOI: 10.1145/2647868.2654935.
- 687 You Q, Luo J, Jin H, Yang J. 2015. Robust image sentiment analysis using progressively trained
688 and domain transferred deep networks. In: *Proceedings of the AAAI Conference on Artificial*
689 *Intelligence*. 29(1). DOI: 10.1609/aaai.v29i1.9179.
- 690 Yang J, She D, Sun M, Cheng M-M, Rosin PL, Wang L. 2018b. Visual sentiment prediction
691 based on automatic discovery of affective regions. *IEEE Transactions on Multimedia*. 20(9):
692 2513-2525. DOI: 10.1109/TMM.2018.2803520.

- 693 Yang J, She D, Lai Y-K, Rosin PL, Yang M-H. 2018a. Weakly supervised coupled networks for
694 visual sentiment analysis. In: *Proceedings of the IEEE Conference on Computer Vision and*
695 *Pattern Recognition*. 7584–7592. DOI: 10.1109/CVPR.2018.00791.
- 696 You Q, Cao L, Jin H, Luo J. 2016. Robust visual-textual sentiment analysis: When attention
697 meets tree-structured recursive neural networks. In: *Proceedings of the 24th ACM International*
698 *Conference on Multimedia*. 1008–1017. DOI: 10.1145/2964284.2964288.
- 699 Kumar A, Garg G. 2019. Sentiment analysis of multimodal twitter data. *Multimedia Tools and*
700 *Applications*. 78: 24103–24119. DOI: 10.1007/s11042-019-7390-1.
- 701 Kumar A, Srinivasan K, Cheng W-H, Zomaya AY. 2020. Hybrid context enriched deep learning
702 model for fine-grained sentiment analysis in textual and visual semiotic modality social data.
703 *Information Processing & Management*. 57: 102141. DOI: 10.1016/j.ipm.2019.102141.
- 704 Xu N, Mao W, Chen G. 2018. A co-memory network for multimodal sentiment analysis. In: *The*
705 *41st International ACM SIGIR Conference on Research & Development in Information*
706 *Retrieval*. 929–932. DOI: 10.1145/3209978.3210093.
- 707 Vo D-T, Zhang Y. 2015. Target-dependent twitter sentiment classification with rich automatic
708 features. In: *Twenty-Fourth International Joint Conference on Artificial Intelligence*. 1347–1353.
709 DOI: 10.5555/2832415.2832437.
- 710 Dong L, Wei F, Tan C, Tang D, Zhou M, Xu K. 2014. Adaptive recursive neural network for
711 target-dependent twitter sentiment classification. In: *Proceedings of the 52nd Annual Meeting of*
712 *the Association for Computational Linguistics (Volume 2: Short Papers)*. 49–54. DOI:
713 10.3115/v1/P14-2009.
- 714 Xue W, Li T. 2018. Aspect based sentiment analysis with gated convolutional networks. In:
715 *Proceedings of the 56th Annual Meeting of the Association for Computational Linguistics*
716 *(Volume 1: Long Papers)*. 2514-2523. DOI: 10.18653/v1/P18-1234.
- 717 Ma Y, Peng H, Cambria E. 2018. Targeted aspect-based sentiment analysis via embedding
718 commonsense knowledge into an attentive LSTM. In: *Proceedings of the AAAI Conference on*
719 *Artificial Intelligence*. 32(1). DOI: 10.1609/aaai.v32i1.12048.
- 720 Chen P, Sun Z, Bing L, Yang W. 2017. Recurrent attention network on memory for aspect
721 sentiment analysis. In: *Proceedings of the 2017 Conference on Empirical Methods in Natural*
722 *Language Processing*. 452–461. DOI: 10.18653/v1/D17-1047.
- 723 Wang S, Mazumder S, Liu B, Zhou M, Chang Y. 2018. Target-sensitive memory networks for
724 aspect sentiment classification. In: *Proceedings of the 56th Annual Meeting of the Association*
725 *for Computational Linguistics (Volume 1: Long Papers)*. 957–967. DOI: 10.18653/v1/P18-1088.
- 726 Yang C, Zhang H, Jiang B, Li K. 2019. Aspect-based sentiment analysis with alternating
727 coattention networks. *Information Processing & Management*. 56: 463–478. DOI:
728 10.1016/j.ipm.2018.12.004.
- 729 Meškelè D, Frasincar F. 2020. ALDONAr: A hybrid solution for sentence-level aspect-based
730 sentiment analysis using a lexicalized domain ontology and a regularized neural attention model.
731 *Information Processing & Management*. 57: 102211. DOI: 10.1016/j.ipm.2020.102211.

- 732 Zhao L, Liu Y, Zhang M, Guo T, Chen L. 2021. Modeling label-wise syntax for fine-grained
733 sentiment analysis of reviews via memory-based neural model. *Information Processing &*
734 *Management*. 58: 102641. DOI: 10.1016/j.ipm.2021.102641.
- 735 Wang K, Shen W, Yang Y, Quan X, Wang R. 2020. Relational graph attention network for
736 aspect-based sentiment analysis. In: *Proceedings of the 58th Annual Meeting of the Association*
737 *for Computational Linguistics*. 3229-3238. DOI: 10.18653/v1/2020.acl-main.295.
- 738 Zhang M, Qian T. 2020. Convolution over hierarchical syntactic and lexical graphs for aspect
739 level sentiment analysis. In: *Proceedings of the 2020 Conference on Empirical Methods in*
740 *Natural Language Processing (EMNLP)*. 3540–3549. DOI: 10.18653/v1/2020.emnlp-main.286.
- 741 Xu H, Liu B, Shu L, Yu PS. 2019. BERT post-training for review reading comprehension and
742 aspect-based sentiment analysis. In: *Proceedings of the 2019 Conference of the North American*
743 *Chapter of the Association for Computational Linguistics: Human Language Technologies*. 1.
744 DOI: 10.18653/v1/N19-1242.
- 745 Sun C, Huang L, Qiu X. 2019. Utilizing BERT for aspect-based sentiment analysis via
746 constructing auxiliary sentence. In: *Proceedings of the 2019 Conference of the North American*
747 *Chapter of the Association for Computational Linguistics: Human Language Technologies,*
748 *Volume 1 (Long and Short Papers)*. 380-385. DOI: 10.18653/v1/N19-1035.
- 749 Khan Z, Fu Y. 2021. Exploiting BERT for multimodal target sentiment classification through
750 input space translation. In: *Proceedings of the 29th ACM International Conference on*
751 *Multimedia*. 3034–3042. DOI: 10.1145/3474085.3475692.
- 752 Liu Y, Ott M, Goyal N, Du J, Joshi M, Chen D, Levy O, Lewis M, Zettlemoyer L, Stoyanov V.
753 2019. Roberta: A robustly optimized bert pretraining approach. *arXiv preprint*
754 *arXiv:1907.11692*.
- 755 Dai J, Yan H, Sun T, Liu P, Qiu X. 2021. Does syntax matter? A strong baseline for Aspect-
756 based Sentiment Analysis with RoBERTa. In: *Proceedings of the 2021 Conference of the North*
757 *American Chapter of the Association for Computational Linguistics: Human Language*
758 *Technologies*. 1816-1829. DOI: 10.18653/v1/2021.naacl-main.146.
- 759 He K, Zhang X, Ren S, Sun J. 2016. Deep residual learning for image recognition. In:
760 *Proceedings of the IEEE Conference on Computer Vision and Pattern Recognition*. 770–778.
761 DOI: 10.1109/CVPR.2016.90.
- 762 Simonyan K, Zisserman A. 2014. Very deep convolutional networks for large-scale image
763 recognition. *arXiv preprint arXiv:1409.1556*.
- 764 Tsai Y-HH, Bai S, Liang PP, Kolter JZ, Morency L-P, Salakhutdinov R. 2019. Multimodal
765 transformer for unaligned multimodal language sequences. In: *Proceedings of the conference.*
766 *Association for Computational Linguistics*. 6558-6569. DOI: 10.18653/v1/P19-1656.
- 767 Ba JL, Kiros JR, Hinton GE. 2016. Layer normalization. *arXiv preprint arXiv:1607.06450*.
- 768 Yu J, Jiang J, Yang L, Xia R. 2020. Improving multimodal named entity recognition via entity
769 span detection with unified multimodal transformer. In: *Proceedings of the 58th Annual Meeting*
770 *of the Association for Computational Linguistics*. 3342-3352. DOI: 10.18653/v1/2020.acl-
771 main.306.

- 772 Chen T, Borth D, Darrell T, Chang S-F. 2014a. Deepsentibank: Visual sentiment concept
773 classification with deep convolutional neural networks. *arXiv preprint arXiv:1410.8586*.
- 774 Zhao F, Wu Z, Long S, Dai X, Huang S, Chen J. 2022. Learning from Adjective-Noun Pairs: A
775 Knowledge-enhanced Framework for Target-Oriented Multimodal Sentiment Classification. In:
776 *Proceedings of the 29th International Conference on Computational Linguistics*. 6784–6794.
- 777 Wang Y, Huang M, Zhu X, Zhao L. 2016. Attention-based LSTM for aspect-level sentiment
778 classification. In: *Proceedings of the 2016 Conference on Empirical Methods in Natural*
779 *Language Processing*. 606–615. DOI: 10.18653/v1/D16-1058.
- 780 Fan F, Feng Y, Zhao D. 2018. Multi-grained attention network for aspect-level sentiment
781 classification. In: *Proceedings of the 2018 Conference on Empirical Methods in Natural*
782 *Language Processing*. 3433–3442. DOI: 10.18653/v1/D18-1380.
- 783 Devlin J, Chang M-W, Lee K, Toutanova K. 2018. Bert: Pre-training of deep bidirectional
784 transformers for language understanding. *arXiv preprint arXiv:1810.04805*.
- 785 Lu J, Batra D, Parikh D, Lee S. 2019. Vilt: Pretraining task-agnostic visiolinguistic
786 representations for vision-and-language tasks. In: *Proceedings of the 33rd International*
787 *Conference on Neural Information Processing Systems*. 13-23. DOI: 10.5555/3454287.3454289.
- 788

Table 1 (on next page)

Representative examples of ABMSA.

Given an image, a text, and an unspecified number of aspects, we aim to predict the sentiment polarity of each aspect.

1 **Table 1:** Representative examples of ABMSA. Given an image, a text, and an unspecified
2 number of aspects, we aim to predict the sentiment polarity of each aspect.

	Image	Text	Aspect	Output
(a)		Taylor posing with her Taylor Swift Award at the # BMIPopAwards	Taylor	(Taylor, Positive)
(b)		RT @ ESPN Numbers : Everyone reacting to Percy Harvin being traded to the JETS . . .	Percy Harvin JETS	(Percy Harvin, Negative) (JETS, Neutral)

3

Table 2 (on next page)

The basic statistics of two TWITTER datasets.

1

Table 2: The basic statistics of two TWITTER datasets.

	TWITTER-2015			TWITTER-2017		
	Train	Dev	Test	Train	Dev	Test
Positive	928	303	317	1508	515	493
Negative	368	149	113	416	144	168
Neutral	1883	670	607	1638	517	573
Total	3179	1122	1037	3562	1176	1234
Avg Aspects	1.348	1.336	1.354	1.410	1.439	1.450
Words	9023	4238	3919	6027	2922	3013
Avg Length	16.72	16.74	17.05	16.21	16.37	16.38

2

Table 3 (on next page)

Experimental results on TWITTER-2015 and TWITTER-2017 datasets using different unimodal and multimodal methods in the ABMSA task.

1 **Table 3:** Experimental results on TWITTER-2015 and TWITTER-2017 datasets using different
 2 unimodal and multimodal methods in the ABMSA task.

Method	TWITTER-2015		TWITTER-2017	
	Acc	Macro-F1	Acc	Macro-F1
Image Only				
Res-Target	59.88	46.48	58.59	53.98
Text Only				
AE-LSTM	70.30	63.43	61.67	57.97
MGAN	71.17	64.21	64.75	61.46
BERT	74.15	68.86	68.15	65.23
RoBERTa	76.28	71.36	69.77	68.00
Text and Image				
MIMN	71.84	65.69	65.88	62.99
ESAFN	73.38	67.37	67.83	64.22
ViLBERT	73.76	69.85	67.42	64.87
TomBERT	77.15	71.75	70.34	68.03
SaliencyBERT	77.03	72.36	69.69	67.19
CapBERT	78.01	73.25	69.77	68.42
KEF-TomBERT	78.68	73.75	72.12	69.96
KEF-SaliencyBERT	78.15	73.54	71.88	68.96
CapRoBERTa	77.82	73.38	71.07	68.57
KEF-TomRoBERTa	78.75	73.94	72.18	70.21
TISRI (Ours)	78.50	74.42	72.53	71.40

3

Table 4(on next page)

Ablation study of TISRI.

1

Table 4: Ablation study of TISRI.

Method	TWITTER-2015		TWITTER-2017	
	Acc	Macro-F1	Acc	Macro-F1
TISRI	78.50	74.42	72.53	71.40
TISRI w/o IFF	76.57	72.22	71.07	69.74
TISRI w/o IFAR	76.37	72.54	70.02	68.24
TISRI w/o MFRI	77.82	73.85	70.75	68.76
TISRI w/o IFF & IFAR & MFRI	76.28	71.79	68.07	66.86

2

Table 5 (on next page)

Case study of RoBERTa, CapRoBERTa, and TISRI.

✓ and ✗ denote the correct and incorrect predictions, respectively.

1 **Table 5:** Case study of RoBERTa, CapRoBERTa, and TISRI. ✓ and ✗ denote the correct and
 2 incorrect predictions, respectively.

Image				
Text	(a) OKC evens the series ! Kevin Durant 's 41 points lead [Thunder] _{Positive} to 111 - 97 victory over Spurs in Game 4 .	(b) @ Soundkartell did an Interview with @ [tomklose] _{Positive} at @ spotfestival and it was very kind . We talked about @ SpotifyDE	(c) RT @ juventusfcen : Two special memories # OnThisDay : a [UEFA Cup] _{Positive} title in 1977 and our 16th Scudetto in 1975 .	(d) Some of that Dodger baseball * □ @ [alyssajacinto] _{Positive}
Image Gate	0.703	0.648	0.559	0.478
Top-k ANPs	clean air holy cross excellent team tough race victorious team	handsome smile christian heritage stupid face handsome kid clean teeth	poor performance successful team holy angels fresh meat fancy dress	stunning beauty hot girls pretty girls dark skin sexy girls
Label	(Thunder, Positive)	(tomklose, Positive)	(UEFA Cup, Positive)	(alyssajacinto, Positive)
RoBERTa	(Thunder, Positive ✓)	(tomklose, Positive ✓)	(UEFA Cup, Neutral ✗)	(alyssajacinto, Positive ✓)
CapRoBERTa	(Thunder, Neutral ✗)	(tomklose, Neutral ✗)	(UEFA Cup, Neutral ✗)	(alyssajacinto, Neutral ✗)
TISRI (Ours)	(Thunder, Positive ✓)	(tomklose, Positive ✓)	(UEFA Cup, Positive ✓)	(alyssajacinto, Positive ✓)

3

Table 6 (on next page)

Error cases of TISRI.

1

Table 6: Error cases of TISRI.

Image			
Text	(a) Petition to have [Jessica Lange] ^{Neutral} come back for American Horror Story season 6	(b) This morning @ SheilaG Craft hosted a brunch amp poured into our [WILD Women] ^{Positive} to honor them for their leadership in 2014 !	(c) RT @ NYRangers : OFFICIAL : [Martin] ^{Negative} St . Louis announces retirement from the National Hockey League . # NYR
Image Gate	0.590	0.494	0.433
Top-k ANPs	laughing baby crazy cat crazy face poor cat funny baby	awesome cake little tree colorful cake great food jolly christmas	excited crowd ill child excited student holy cross amazing race
Label	(Jessica Lange, Neutral)	(WILD Women, Positive)	(Martin, Negative)
TISRI (Ours)	(Jessica Lange, Positive X)	(WILD Women, Neutral X)	(Martin, Neutral X)

2

Figure 1

The overview of Text-Image Semantic Relevance Identification (TISRI) model architecture.

TISRI consists of four modules: Unimodal Feature Extraction Module, Multimodal Feature Relevance Identification Module, Aspect-Multimodal Feature Interaction Module, and Multimodal Feature Fusion Module.

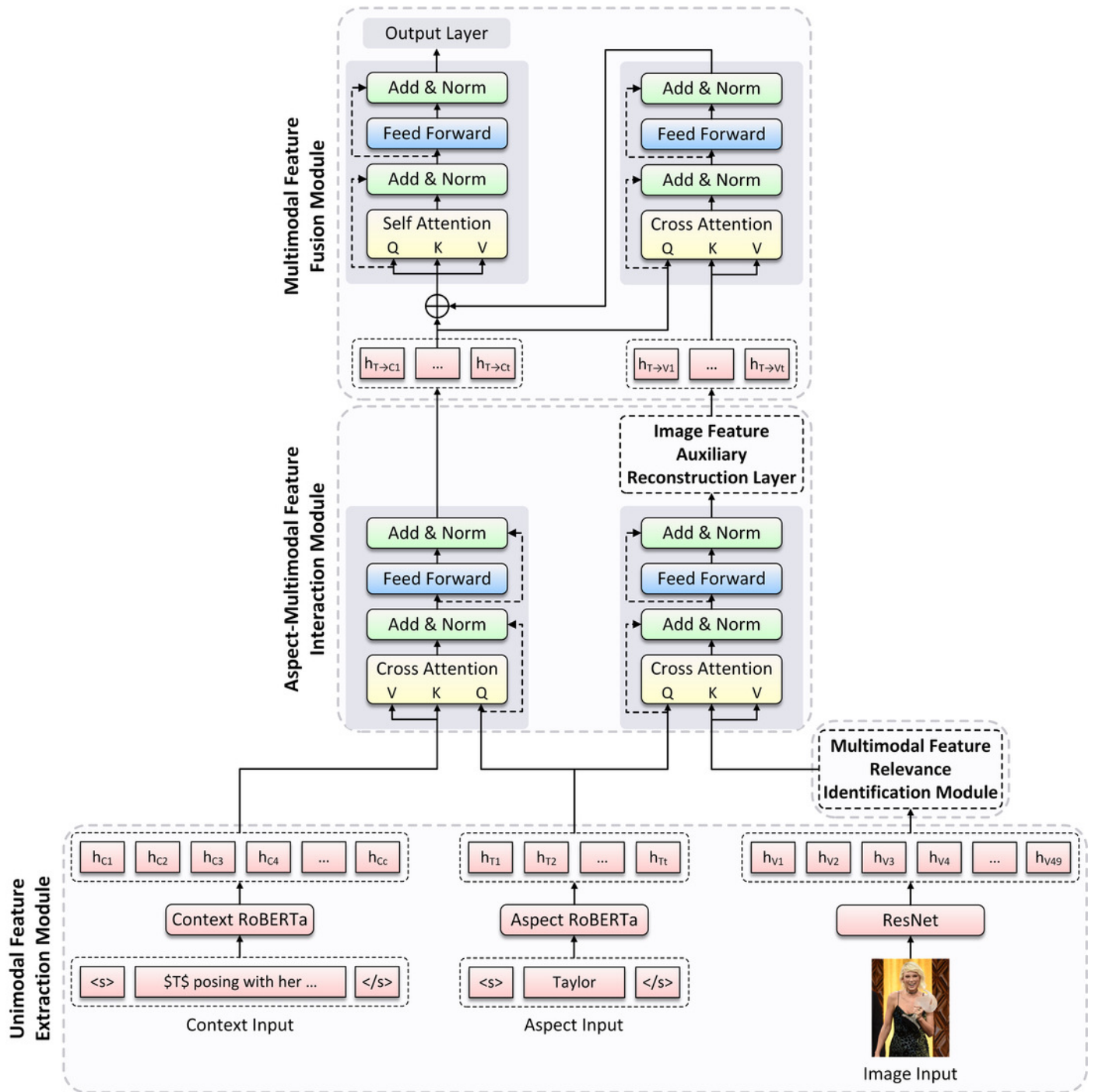


Figure 2

The overview of Multimodal Feature Relevance Identification (MFRI) Module architecture.

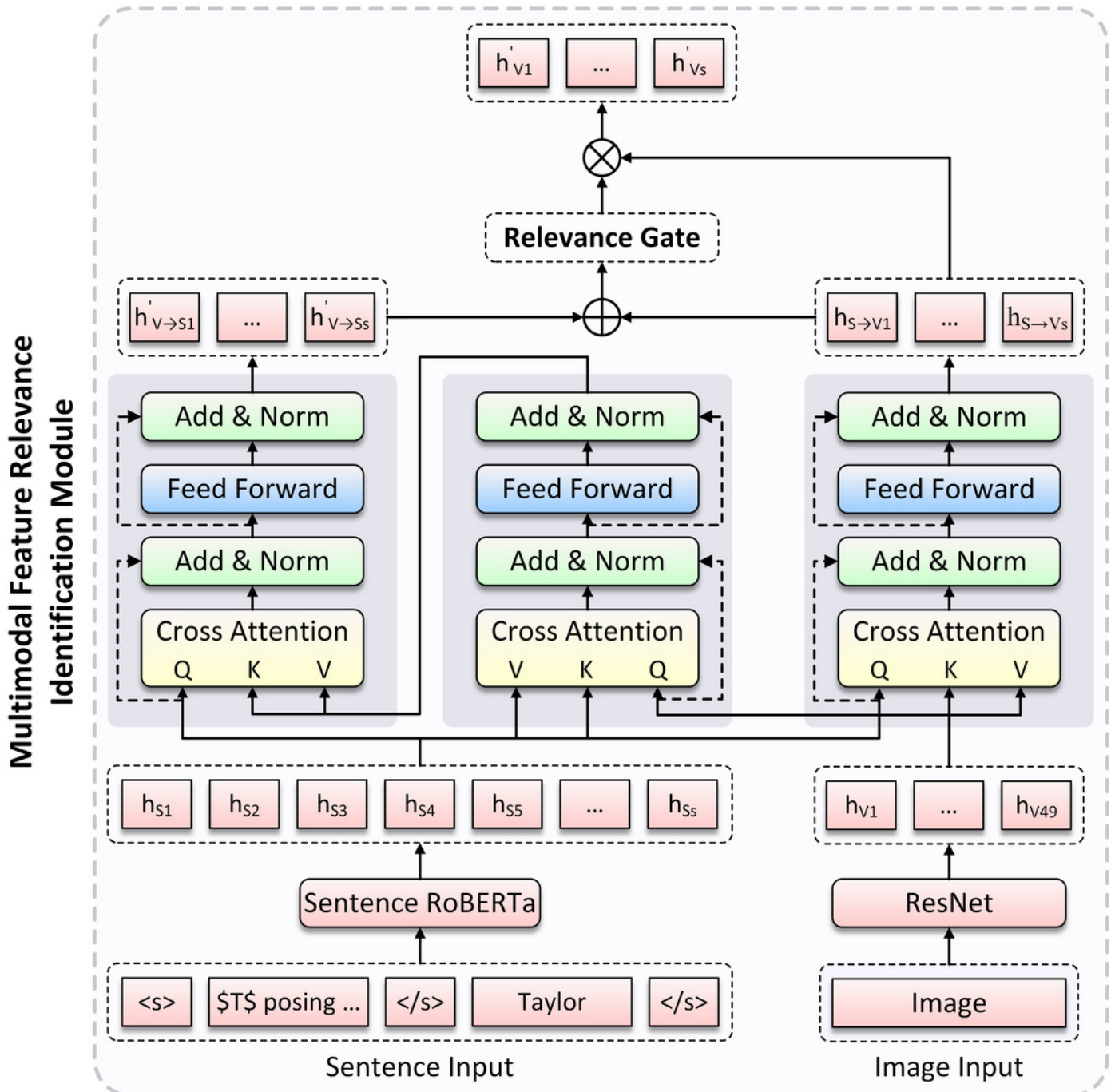


Figure 3

The overview of Image Feature Auxiliary Reconstruction (IFAR) Layer architecture.

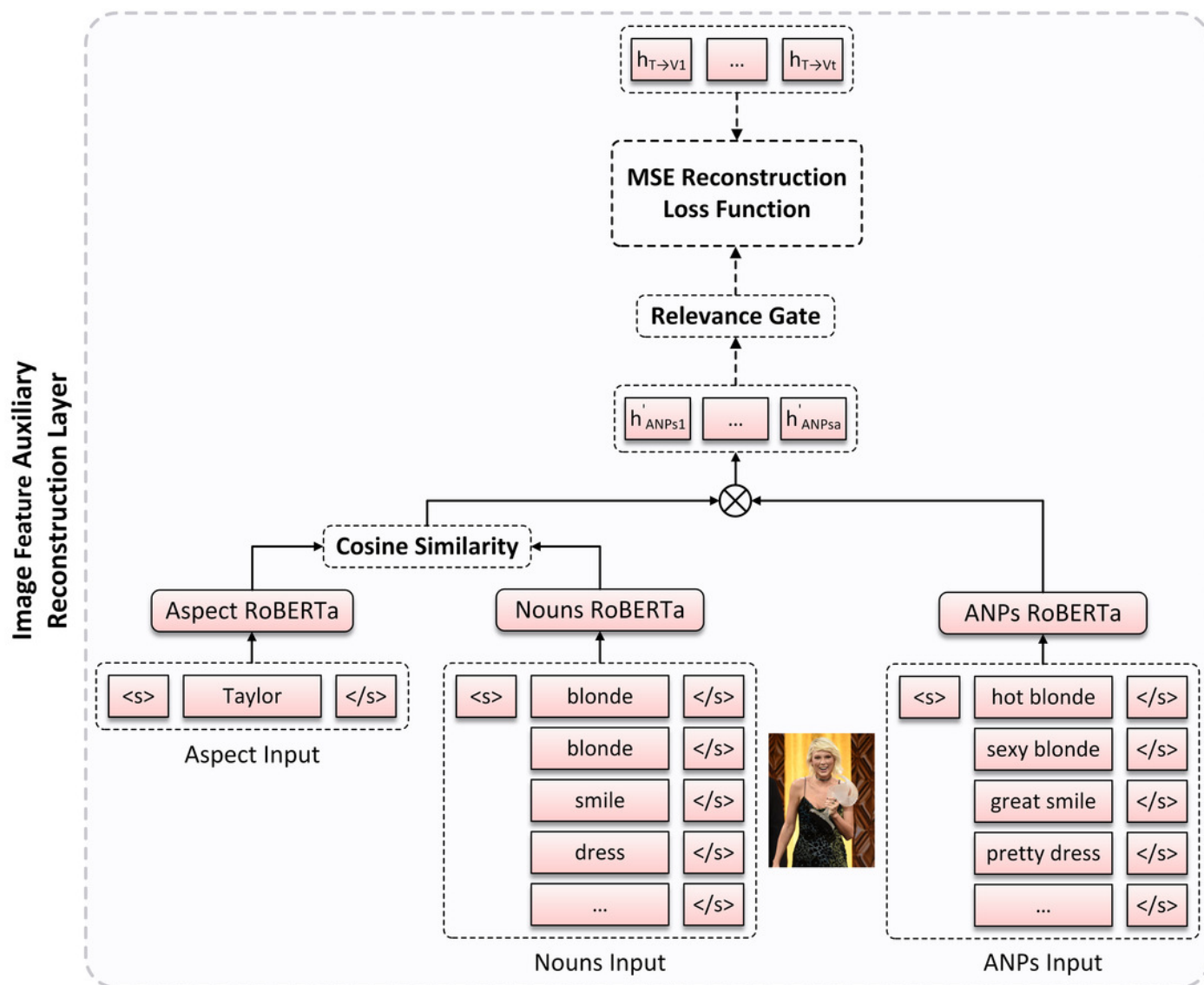


Figure 4

Effect of epoch on TWITTER-2015

Effect of epoch on model Accuracy and Macro-F1.

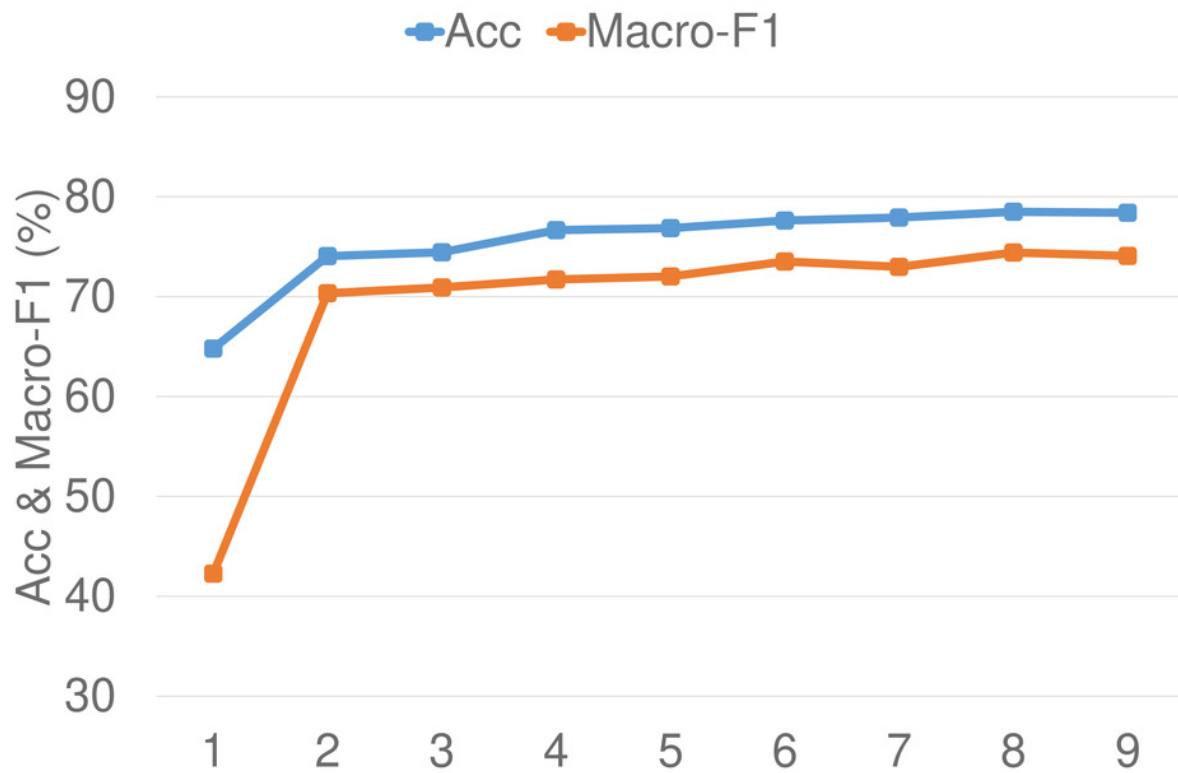


Figure 5

Effect of epoch on TWITTER-2017

Effect of epoch on model Accuracy and Macro-F1.

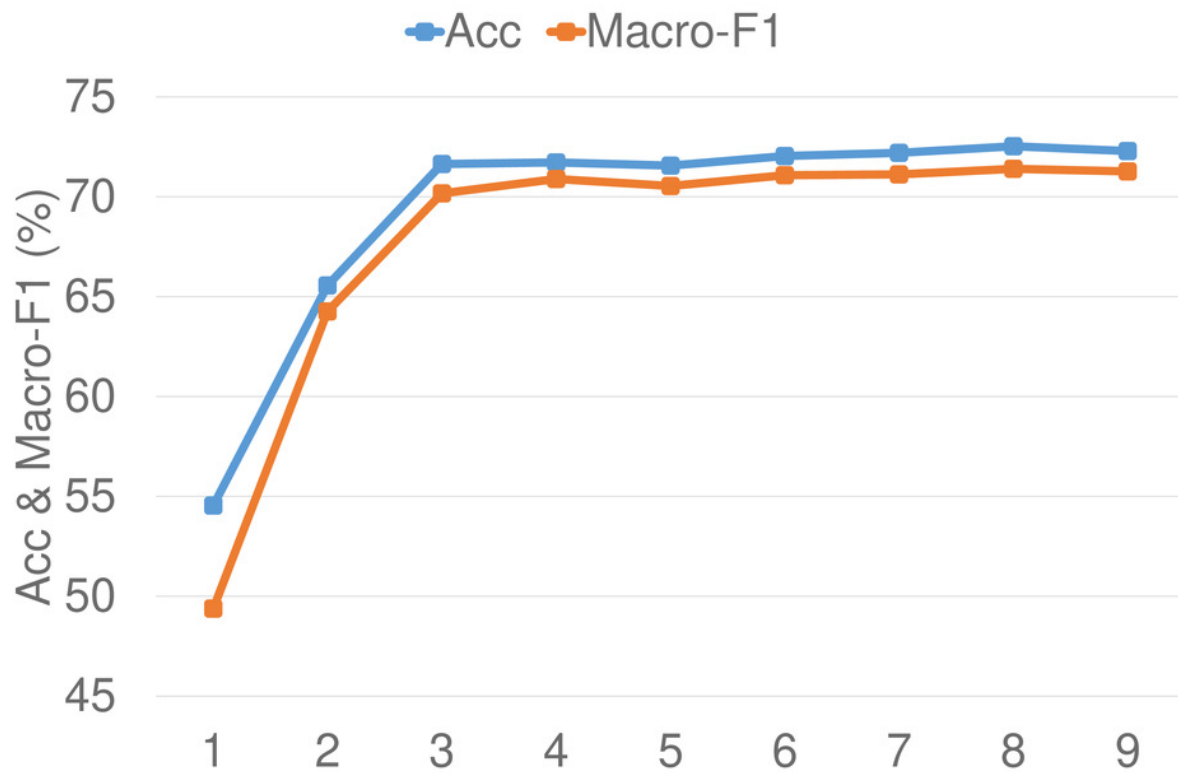


Figure 6

Effect of batch size on TWITTER-2015

Effect of batch size on model Accuracy and Macro-F1.

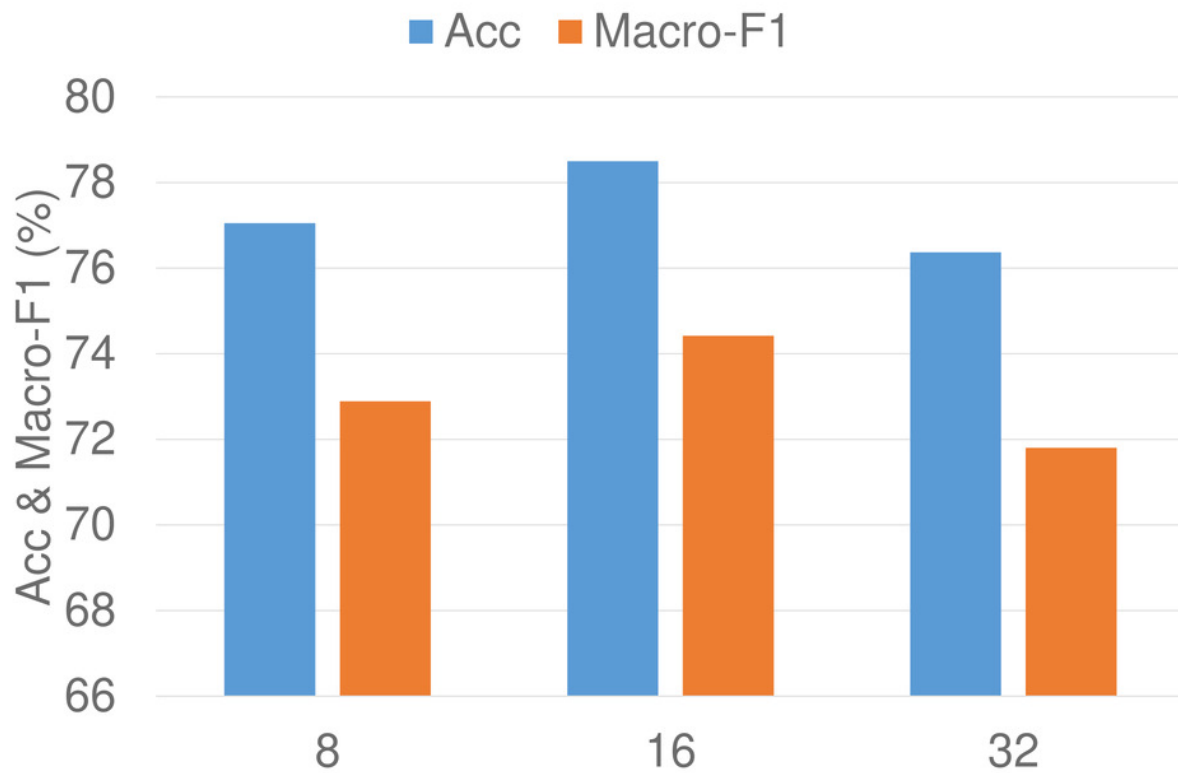


Figure 7

Effect of batch size on TWITTER-2017

Effect of batch size on model Accuracy and Macro-F1.

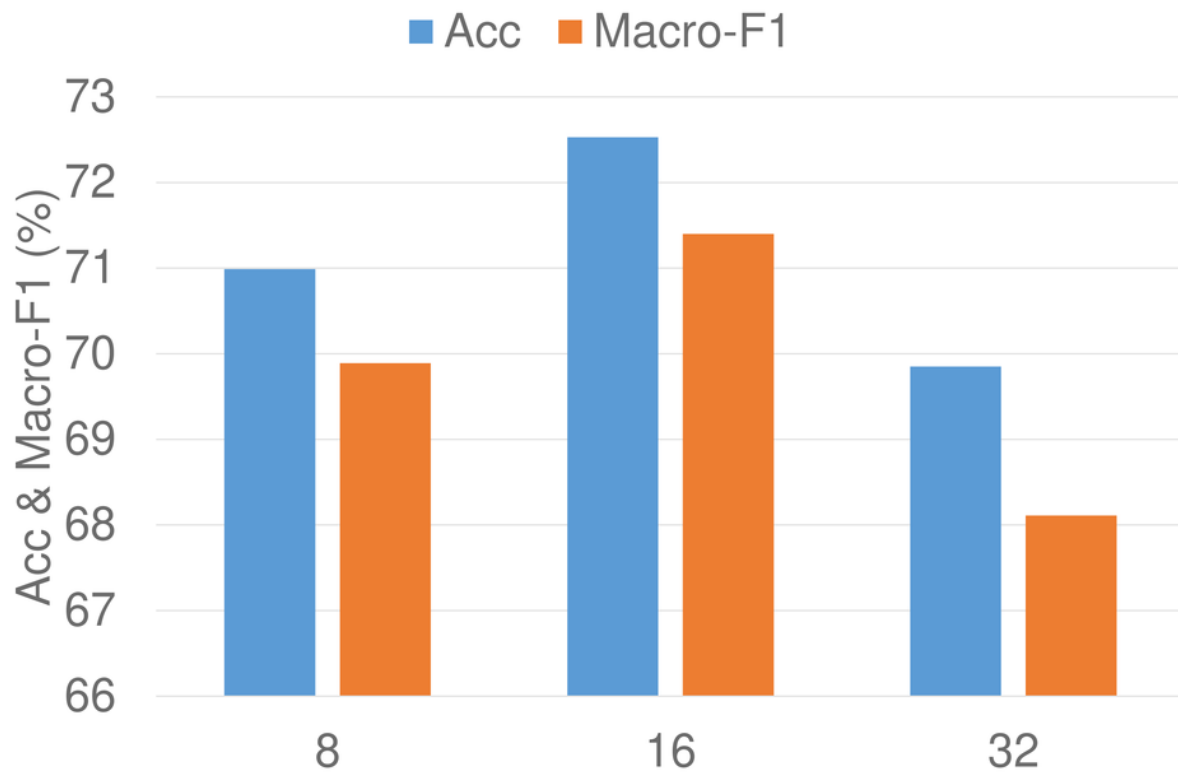


Figure 8

Effect of k on TWITTER-2015

Effect of k on model Accuracy and Macro-F1.

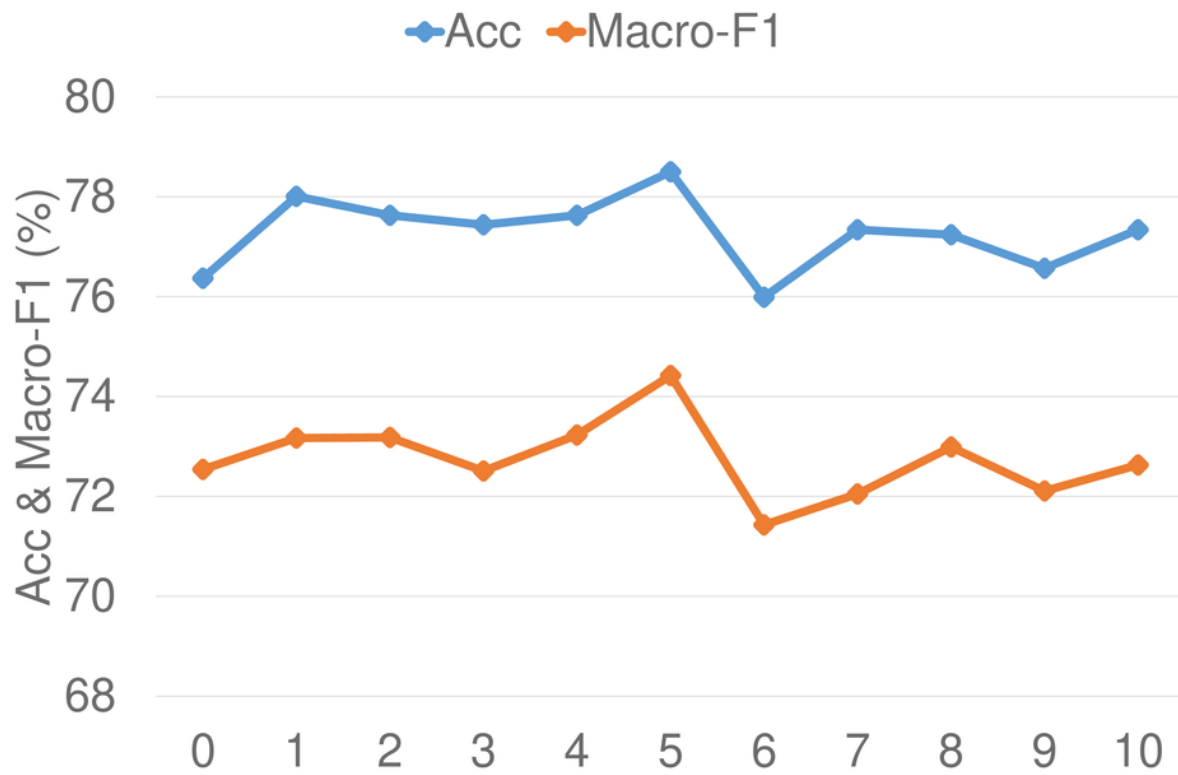


Figure 9

Effect of k on TWITTER-2017

Effect of k on model Accuracy and Macro-F1.

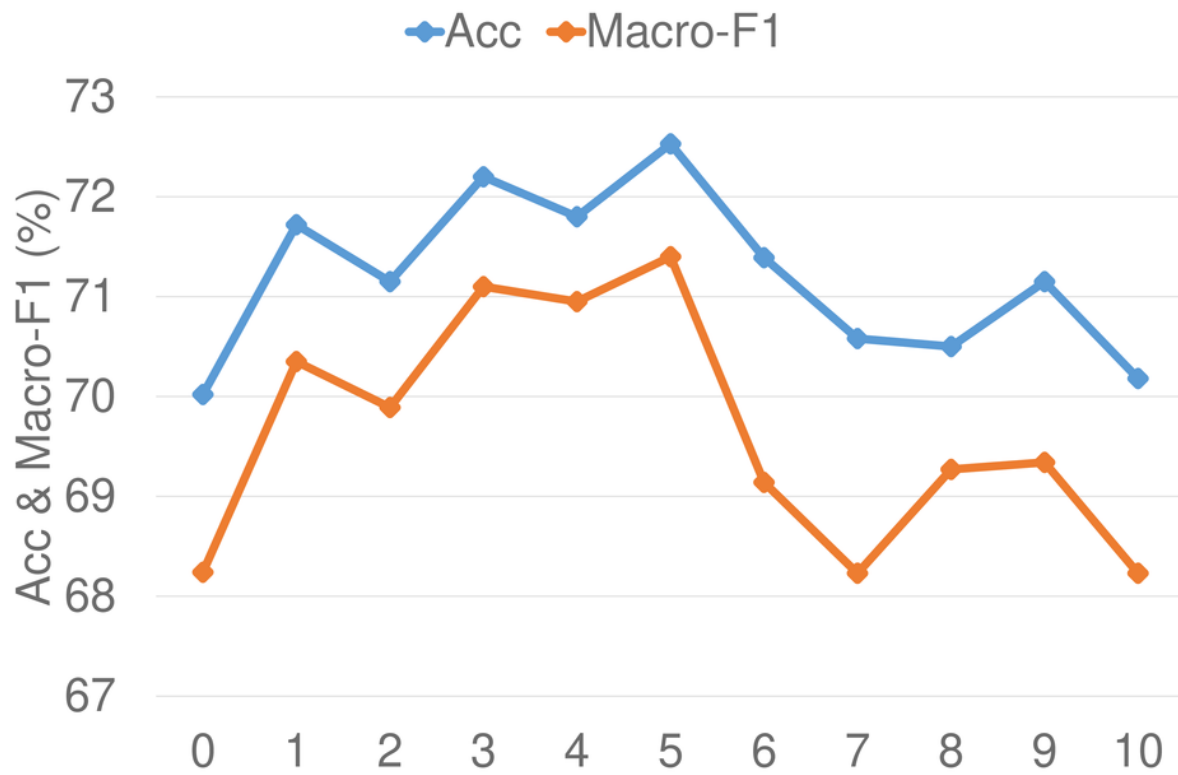


Figure 10

Effect of λ on TWITTER-2015

Effect of λ on model Accuracy and Macro-F1.

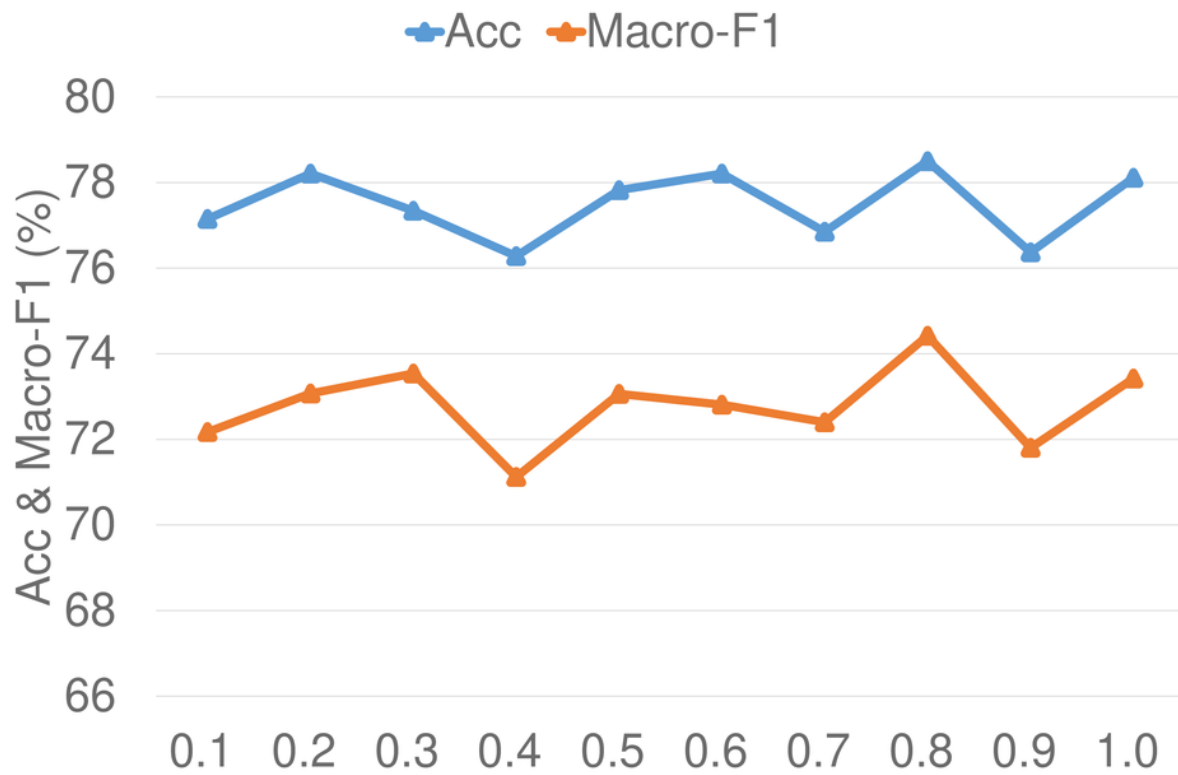


Figure 11

Effect of λ on TWITTER-2017

Effect of λ on model Accuracy and Macro-F1.

